

# Atomic Layer Deposition of Undoped TiO<sub>2</sub> Exhibiting *p*-Type Conductivity

Andrei T. Iancu,<sup>\*,†</sup> Manca Logar,<sup>†</sup> Joonsuk Park,<sup>‡</sup> and Fritz B. Prinz<sup>†,‡</sup>

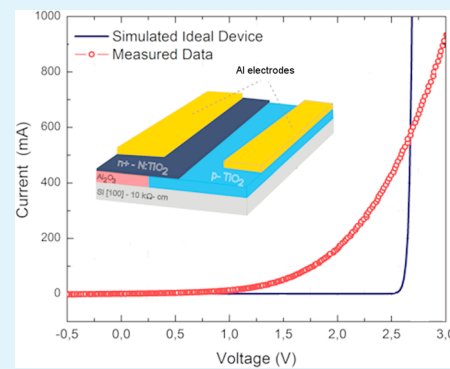
<sup>†</sup>Department of Mechanical Engineering, Stanford University, Stanford, California 94305, United States

<sup>‡</sup>Department of Materials Science and Engineering, Stanford University, Stanford, California 94305, United States

## Supporting Information

**ABSTRACT:** With prominent photocatalytic applications and widespread use in semiconductor devices, TiO<sub>2</sub> is one of the most popular metal oxides. However, despite its popularity, it has yet to achieve its full potential due to a lack of effective methods for achieving *p*-type conductivity. Here, we show that undoped *p*-type TiO<sub>2</sub> films can be fabricated by atomic layer deposition (ALD) and that their electrical properties can be controlled across a wide range using proper postprocessing anneals in various ambient environments. Hole mobilities larger than 400 cm<sup>2</sup>/(V·s) are accessible superseding the use of extrinsic doping, which generally produces orders of magnitude smaller values. Through a combination of analyses and experiments, we provide evidence that this behavior is primarily due to an excess of oxygen in the films. This discovery enables entirely new categories of TiO<sub>2</sub> devices and applications, and unlocks the potential to improve existing ones. TiO<sub>2</sub> homojunction diodes fabricated completely by ALD are developed as a demonstration of the utility of these techniques and shown to exhibit useful rectifying characteristics even with minimal processing refinement.

**KEYWORDS:** atomic layer deposition, titanium dioxide, *p*-type conductivity, *p*–*n* homojunction diode, Hall effect, X-ray diffraction, X-ray photoelectron spectroscopy, transmission electron microscopy



## INTRODUCTION

Titanium dioxide (TiO<sub>2</sub>) is a versatile material with a diverse set of existing applications. Traditionally, it has been used as an industrial pigment as well as an efficient ultraviolet absorber in sunscreen.<sup>1</sup> More recently, it has been employed as a photocatalyst for sterilizing, deodorizing, antifouling and other similar processes.<sup>2–4</sup> TiO<sub>2</sub> thin films have been researched as potential high dielectric constant layers in dynamic random-access memory<sup>5,6</sup> and metal-oxide-semiconductor field effect transistor devices<sup>7</sup> as well as resistive switching layers in resistive random-access memory.<sup>8–10</sup> Promising applications in solar water splitting devices as a photoanode coating<sup>11–13</sup> and numerous uses in photovoltaic architectures<sup>14–16</sup> have also been investigated by a number of groups. These examples are just a few of the current, prominent uses of the material.

Although TiO<sub>2</sub> is a relevant material with a significant amount of research that has been done toward its fundamental characterization and its implementation in devices, there are few studies on its potential for native *p*-type conductivity. This has limited its application to heterojunction architectures and oxidation-based chemical processes. Though many have attempted to *p*-type dope the material system with elements such as Cr, Mn, Zn, Al, Ni and so on with some success, such doping negatively affects the electrical properties of the film, especially the carrier mobility, resulting in poor device performance.<sup>17–20</sup> Some simulations and a scant few experi-

ments have suggested the possibility of fabricating undoped *p*-type TiO<sub>2</sub> but high temperatures in excess of 800 °C were necessary for the synthesis, and this limits the potential applications.<sup>21–23</sup>

In this work, we establish a technique for directly fabricating *p*-type TiO<sub>2</sub> films on silicon by atomic layer deposition (ALD) at temperatures as low as 200 °C. The films are additionally annealed in a wide range of temperatures and environments then characterized in order to explore the array of material properties that are achievable and the underlying physical factors that produce them. We show that one can precisely tailor *p*-type TiO<sub>2</sub> electrical characteristics across many orders of magnitude enabling a variety of novel devices and applications. Transparent TiO<sub>2</sub> junctions for use in low cost light-emitting diodes and photovoltaics become feasible due to hole mobilities in excess of 400 cm<sup>2</sup>/(V·s) and hole concentrations greater than 10<sup>19</sup> cm<sup>-3</sup>. Enhancement of photocatalytic activity, through mechanisms such as surface carrier depletion and extreme work function tuning, is now viable. New pathways for resistive switching in the material are also possible. These are just a subset of the new, enabled opportunities. As a demonstration, TiO<sub>2</sub> homojunction diodes were fabricated using the developed processes and shown to

Received: October 18, 2014

Accepted: January 8, 2015

Published: January 8, 2015

exhibit rectifying behavior capable of immediate incorporation into device architectures. To the best of our knowledge, this is the first reported instance of the synthesis of TiO<sub>2</sub> homojunction diodes by ALD.

## MATERIALS AND METHODS

Undoped, float-zone (FZ) single-crystal silicon wafer substrates acquired from Silicon Quest International were used for sample fabrication. The wafers were 100 mm in diameter with a polished (100) orientation surface, a thickness of 500  $\mu\text{m}$  and a resistivity greater than 10 000  $\Omega\cdot\text{cm}$ . This material was used due to the need for a high resistivity substrate to enable the accurate measurement of the thin film electrical properties as well as its purity and widespread use in device fabrication. Our observations indicate that substrate characteristics, primarily composition and topography, can cause large variations in deposited film properties such that TiO<sub>2</sub> films deposited at identical conditions on sapphire, glass and silicon will exhibit radically different behavior.

The wafers were first dipped in a 50 °C 5:1:1 H<sub>2</sub>O:NH<sub>4</sub>OH:H<sub>2</sub>O<sub>2</sub> solution for 10 min to remove all organic contaminants. They were then dipped in a 70 °C 5:1:1 H<sub>2</sub>O:HCl:H<sub>2</sub>O<sub>2</sub> solution for 10 min to remove all ionic contaminants. Finally, they were rinsed with deionized water and dried using a spin-rinse drier then placed into a Cambridge Nanotech Savannah ALD system.

ALD is a monolayer-by-monolayer deposition technique in which a set of chemical precursors are sequentially pulsed through a reactor containing the substrate. The precursor chemicals are not allowed to react with each other but are introduced, allowed to interact with the substrate then purged in a cyclic fashion. With the proper choice of precursor chemistry and reactor conditions, the desired film grows one monolayer per cycle, providing accurate control over the final film thickness based only on the total number of deposition cycles performed. The deposition pressure depends on the system employed but it was held at 1 mTorr for this set of experiments. An argon carrier gas was used to aid precursor delivery to the reactor. Tetrakis-(dimethylamido) titanium (TDMAT), Ti(N(CH<sub>3</sub>)<sub>2</sub>)<sub>4</sub>, was heated to 75 °C and provided the Ti component of the desired film. Deionized water vapor at room temperature served as the oxidant.

Three TiO<sub>2</sub> deposition conditions were chosen: (1) ~30 nm TiO<sub>2</sub> deposited at 200 °C, (2) ~30 nm TiO<sub>2</sub> deposited at 250 °C and (3) ~30 nm N-doped TiO<sub>2</sub> deposited at 250 °C. The N-doped TiO<sub>2</sub> was fabricated with a 1 atomic % doping level by overheating the titanium precursor to 100 °C such that slight precursor decomposition resulted in some nitrogen retention in the final film. The purpose of the nitrogen doping was for comparison to other doped TiO<sub>2</sub> films and to ensure initial *n*-type conductivity for that sample set.<sup>24</sup> The as-deposited, wafer-scale thickness uniformity of the films was excellent with a maximum value of 1% across all samples. ALD growth rates of 0.39 and 0.40 Å per cycle were observed at 200 and 250 °C, respectively. Literature indicates increased ALD growth rates for temperatures in excess of 200 °C,<sup>25</sup> but we did not encounter these until ~270 °C for our reactor configuration. We have observed significant ALD process changes even with simple system modifications, so this was not surprising.

A total of eight samples at each deposition condition were prepared. One of the samples was left as deposited while the other seven were annealed for 6 min at temperatures ranging from 400 to 1000 °C in steps of 100 °C. The 200 and 250 °C undoped samples were annealed in a flow of 10 slpm of N<sub>2</sub>. Some undoped samples were also annealed in a flow of 10 slpm of O<sub>2</sub> but no significant differences were observed, so only the N<sub>2</sub> anneal data is presented. The N-doped samples were annealed in a flow of 10 slpm of O<sub>2</sub>. Annealing the N-doped samples in 10 slpm of N<sub>2</sub> resulted in persistent *n*-type behavior, which was not of interest, so that data is not presented.

All 24 samples were characterized in an identical fashion. A Woollam M-2000 ellipsometer was used to obtain high resolution film thickness measurements. A PHI VersaProbe II scanning X-ray photoelectron spectroscopy (XPS) system was employed to obtain film composition data. A PANalytical X'Pert PRO X-ray diffraction

(XRD) system was utilized to obtain film structural properties. An Ecopia HMS-3000 Van Der Pauw Hall measurement system was applied to measure the film electrical properties. Scanning electron microscopy (SEM, FEI Magellan XHR) was used to obtain high resolution surface topography images. Transmission electron microscopy (TEM, FEI Titan) was used for film cross-sectional imaging and additional composition/phase analysis. For the electron energy loss spectroscopy (EELS) spectra acquisition, a convergence semiangle of 9.6 mrad and collection semiangle of 24 mrad were used. The spectra were acquired using the line profile feature from the Titan Imaging and Analysis (TIA) software applied to the sample region of interest. Spectra were collected at a 1 nm interval. The spectrum processing for elemental quantification was performed with the Digital Micrograph EELS analysis software suite. Fourier-log deconvolution processing was employed to remove the plural scattering. The background of the spectra was subtracted using a power-law model. The quantification of the oxygen and titanium elements in the cross-sectional TiO<sub>2</sub> films was calculated from the EELS core loss region. The element concentrations were obtained by Hartree–Slater and hydrogenic calculation of the ionization cross sections for the Titanium-L and Oxygen-K edges, respectively.

## RESULTS AND DISCUSSION

The TiO<sub>2</sub> film thickness as a function of annealing temperature was analyzed by spectroscopic ellipsometry, as shown in Figure 1. The as-deposited film thickness is illustrated by the left-most

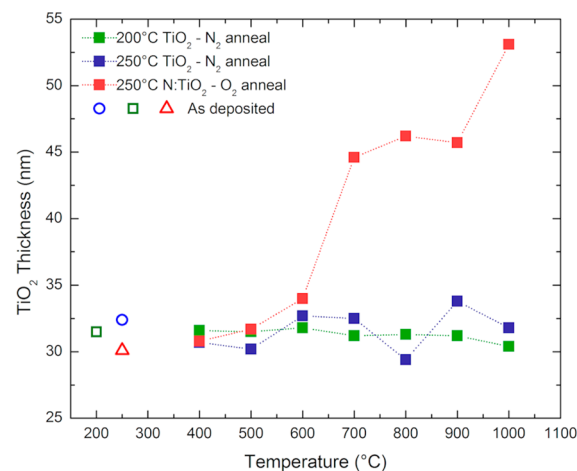


**Figure 1.** TiO<sub>2</sub> thickness of O<sub>2</sub> annealed 250 °C deposited N:TiO<sub>2</sub>, N<sub>2</sub> annealed 250 °C deposited TiO<sub>2</sub> and N<sub>2</sub> annealed 200 °C deposited TiO<sub>2</sub> films as a function of annealing temperature with as deposited measurements shown as the left-most data points.

data points of the figure at the appropriate ALD deposition temperatures and the remainder of the data points are for the anneals in the respective ambient gas flows. Only annealing in oxygen ambient has a significant effect on the thickness and that effect does not become pronounced until temperatures in excess of 700 °C.

To understand the origin of the large, measured increases in film thickness with O<sub>2</sub> annealing, an SEM study (Figure 2) in which the electron beam and detector were configured to provide topographical information with a high degree of surface sensitivity was performed. At the 700 °C temperature at which the thickness of the oxygen annealed films rapidly increases, there is a significant jump in the crystallinity of the material. At that temperature, small gaps in the film begin to appear due to the conversion of amorphous TiO<sub>2</sub> into the higher density crystalline phases of the material. In contrast, SEM analysis of

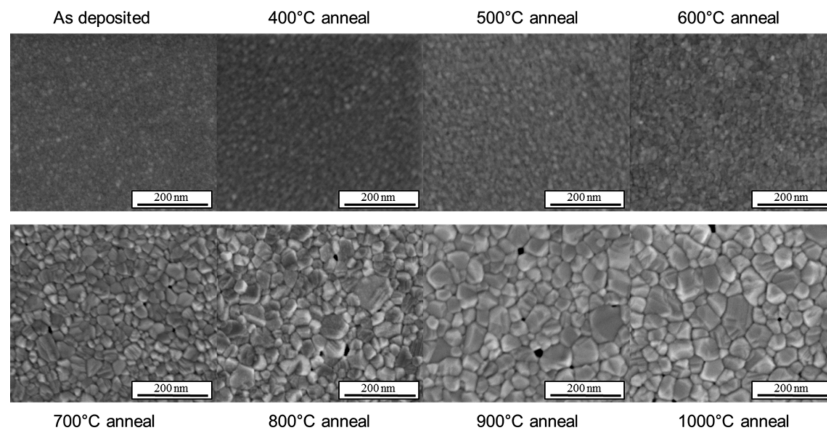


**Figure 2.** Surface topography SEM analysis of N:TiO<sub>2</sub> films as a function of oxygen annealing temperature.

the N<sub>2</sub> annealed samples (Figure S1, Supporting Information) shows smoother surfaces and only moderate crystallinity increases even at higher temperature conditions. Additional data provided by a cross-sectional TEM analysis (Figure S2, Supporting Information) corroborates the SEM results but also indicates that an interfacial silicon oxide layer that thickens at higher O<sub>2</sub> annealing temperatures forms as well. Thus, some of the thickness increases seen in the ellipsometry results are due to the increased surface roughness of the film and the contributions of the SiO<sub>x</sub> at O<sub>2</sub> annealing temperatures of 700 °C and above. However, a large, but difficult to accurately quantify, fraction of the thickness increase is due to the aforementioned increase in grain size and overall crystallinity of the material with higher O<sub>2</sub> annealing temperatures. As will be later demonstrated, the *p*-type behavior of the material persists even through these significant morphological changes.

Examining XRD data from the ALD films deposited at 250 °C in Figure 3a,b, it can be inferred that the as-deposited films are primarily amorphous with small rutile crystallite inclusions dispersed throughout. Moreover, there is no significant effect on the film morphology from the 1% nitrogen doping. As the annealing temperature is increased, measurable crystallization begins to occur around 600 °C and accelerates with the rising temperature. From the transient brookite phase peaks measured at temperatures around this 600 °C transition region, it is reasonable to deduce that the amorphous component of the TiO<sub>2</sub> film crystallizes through either direct transformation into the rutile phase or an indirect transformation into the rutile phase with brookite as an intermediate state. Additional data provided by a cross-sectional TEM analysis of grain crystallinity (Figure S3, Supporting Information) reinforces the XRD findings and provides evidence that some small brookite crystallites below the XRD system resolution are present even at the 400 °C annealing temperatures. It is notable that regardless of the ambient process gas, the effects of the annealing on film morphology are similar for the two samples. The brookite XRD peaks do appear at lower temperatures for the undoped TiO<sub>2</sub> annealed in nitrogen. The underlying mechanism behind this result could be attributed to either the nitrogen doping of the oxygen annealed sample or an effect of the annealing process gas itself.

XRD analysis results from the ALD films deposited at 200 °C and annealed in a nitrogen ambient, shown in Figure 3c, are considerably different than those from the 250 °C samples. This indicates that the ALD deposition temperature has a powerful effect on the physical structure of the deposited films.

Most noticeable is the fact that, as deposited, the 200 °C film has both brookite and rutile components dispersed throughout an amorphous matrix. Moreover, the brookite phase persists until higher annealing temperatures but does eventually fully transform to rutile around the expected transition temperature of 800 °C.<sup>26</sup> In the nanoscale size regime, the size of the TiO<sub>2</sub> crystallites has been shown to determine the thermodynamic phase stability.<sup>27</sup> For nanocrystalline TiO<sub>2</sub>, anatase and brookite are the most stable phases at temperatures below 580 °C. However, for a TiO<sub>2</sub> crystallite size above 11 nm, the brookite phase has been shown to be the most thermodynamically stable. Low anatase–brookite transformation energy (11.9 kJ·mol<sup>-1</sup>) can be sufficient for complete transformation of the anatase to its polytypic brookite structure as crystallite size in the films increases above 11 nm.<sup>27</sup> However, despite these initial differences, the final morphology of the film after the very high temperature anneals at 900 and 1000 °C is similar to those of the samples deposited at 250 °C. The strong dependence of TiO<sub>2</sub> annealing crystallization on the initial structure of the films that is seen in these results has also been observed and characterized in more detail in a number of other publications providing additional evidence for the versatility of this material system.<sup>28,29</sup>

Analyzing the electronic properties of the TiO<sub>2</sub> films as a function of annealing temperature using a Hall effect measurement system (Figure 4), the most prominent feature of the data is the predominance of *p*-type conductivity in the samples. With the exception of the as-deposited N-doped sample and the two highest temperature anneals of the 200 °C deposited sample, all samples consistently exhibited *p*-type semiconductor behavior across all measurements. No significant evidence for this effect has been found in published literature for either ALD TiO<sub>2</sub> films or TiO<sub>2</sub> films deposited by any other method. However, single-crystal rutile phase TiO<sub>2</sub> has been shown to exhibit *p*-type conductivity upon certain high temperature anneals designed to produce titanium vacancies in the lattice.<sup>21</sup>

At the 700 °C annealing temperature that was previously shown to represent the onset of rapid film crystallization, the measurement of the electrical properties of the films became significantly more difficult and the error bars in the results highlight this. Since the data were acquired using a Hall Effect system and grain boundary effects are known to cause significant variability in such planar measurements, it is reasonable to assume that this was the case in this set of experiments as well. More focus will be placed on the electrical

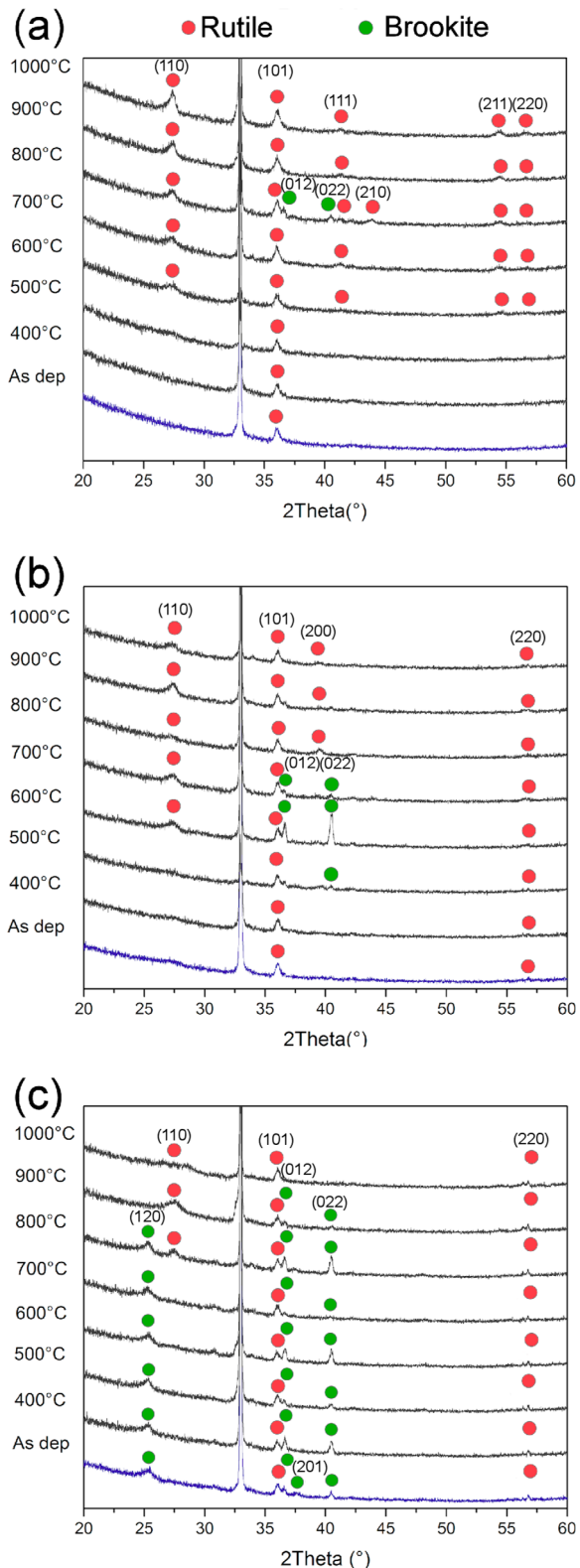


**Figure 3.** XRD analysis of ALD films of (a)  $O_2$  annealed 250 °C deposited N:TiO<sub>2</sub>, (b) N<sub>2</sub> annealed 250 °C deposited TiO<sub>2</sub> and (c) N<sub>2</sub> annealed 200 °C deposited TiO<sub>2</sub> films as a function of annealing temperature.

characteristics at annealing temperatures up to 600 °C because those represent a useful range of achievable properties for subsequent incorporation into various semiconductor devices.

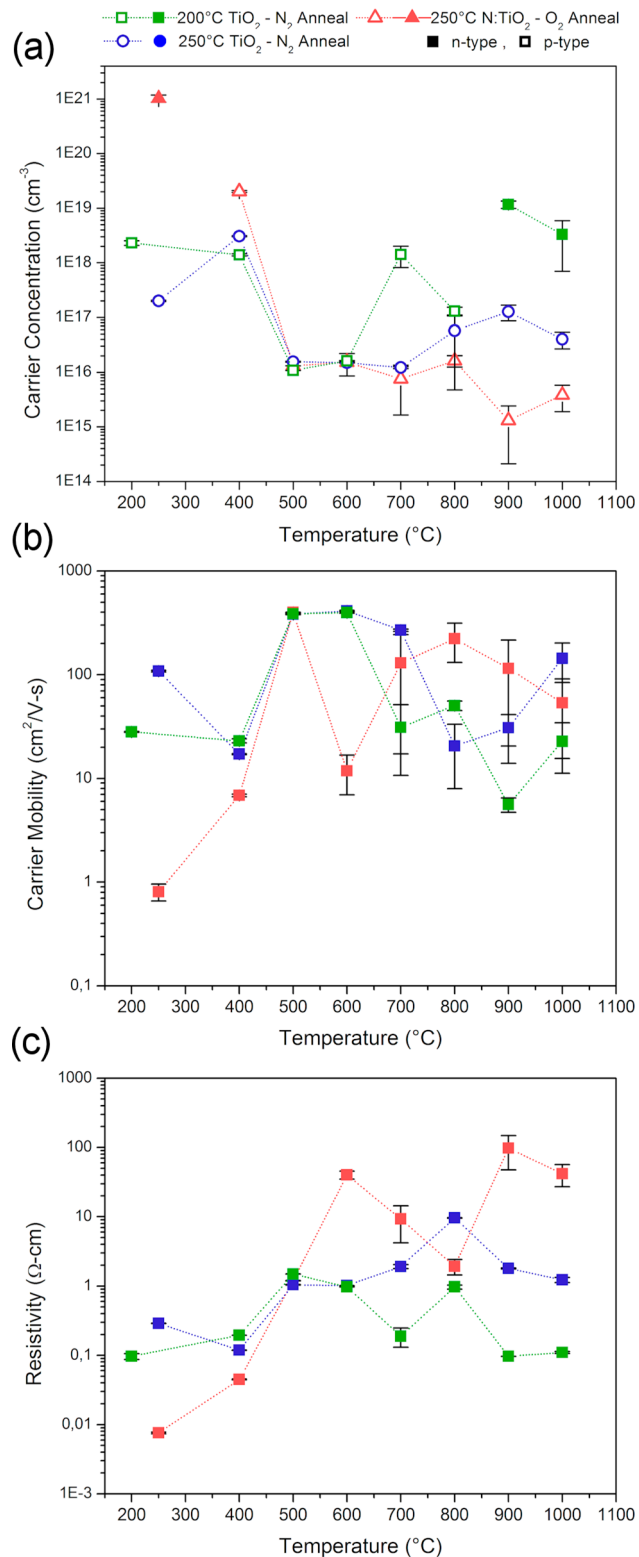


**Figure 4.** Electrical properties of  $O_2$  annealed 250 °C deposited N:TiO<sub>2</sub>, N<sub>2</sub> annealed 250 °C deposited TiO<sub>2</sub> and N<sub>2</sub> annealed 200 °C deposited TiO<sub>2</sub> films as a function of annealing temperature: (a) majority carrier concentration, (b) majority carrier mobility and (c) resistivity.

Regarding the as-deposited properties, the nitrogen-doped film is heavily *n*-type, as expected from previous doping studies. It starts off with a very high majority electron concentration coupled with very low carrier mobility and resistivity. The

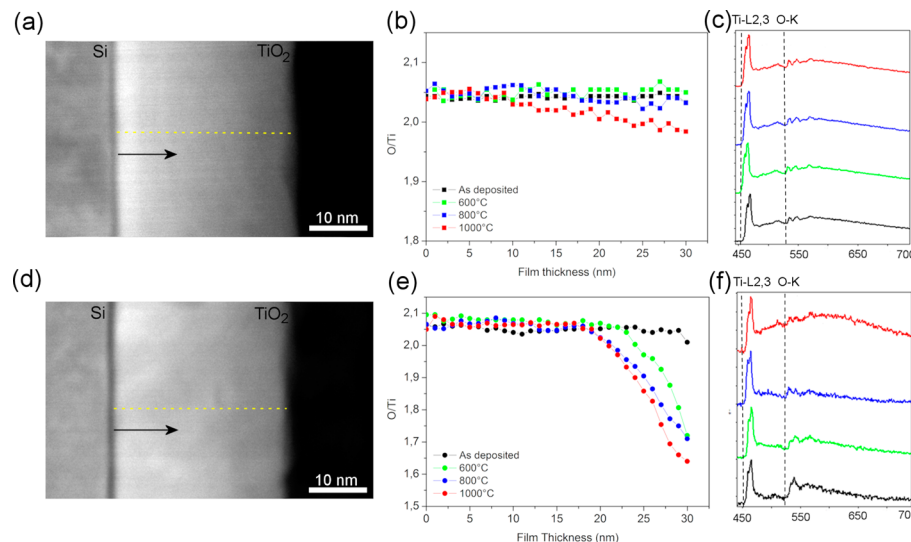


**Figure 5.** STEM-EELS cross-sectional analysis of (a–c)  $O_2$  annealed N:TiO<sub>2</sub> deposited at 250 °C and (d–f) N<sub>2</sub> annealed TiO<sub>2</sub> deposited at 200 °C: (a) dark field STEM image of as deposited N:TiO<sub>2</sub> film, (b) cross-sectional O/Ti concentration profile versus annealing temperature, (c) top surface EELS spectrum versus annealing temperature, (d) dark field STEM image of as-deposited TiO<sub>2</sub> film, (e) cross-sectional O/Ti concentration profile versus annealing temperature and (f) top surface EELS spectrum versus annealing temperature.

undoped films are *p*-type as deposited with moderate majority hole concentrations and higher carrier mobilities. It is notable that the film deposited at 200 °C has a higher hole concentration and subsequently lower mobility and resistivity than the 250 °C film. This result is unexpected but may be attributed to the previous data indicating that it is a more diverse mixture of both brookite and rutile phases within an amorphous matrix.

Upon annealing, the electrical properties of all three sample sets converge at a temperature of 500 °C. At this condition, the values of the carrier concentration, mobility and resistivity for all three sets are virtually identical. This persists for the undoped films at 600 °C but the nitrogen-doped film mobility decreases drastically at this temperature. It is hypothesized that this difference is primarily due to enhanced crystallization of the doped sample at a lower temperature in the oxygen annealing environment because we see similar sharp decreases in mobility at 700 °C temperatures for the undoped samples. The sharp transition from *n*-type to *p*-type behavior in the N-doped samples is due to the rapid loss of nitrogen dopant from the films in the O<sub>2</sub> annealing conditions. The same effect is not observed for N<sub>2</sub> annealing conditions of these N-doped films, which supports the measurements showing the undoped TiO<sub>2</sub> films to be natively *p*-type.

The most important feature of these results is that a large parameter space is accessible for the fabrication of *p*-type TiO<sub>2</sub> with device-tailored properties. The hole concentration can be varied from below 10<sup>16</sup> cm<sup>-3</sup> to over 10<sup>19</sup> cm<sup>-3</sup>. The mobility can be increased to over 400 cm<sup>2</sup>/(V·s) and the resistivity can range from 0.01 to 100 Ω·cm. This provides the device designer a certain amount of flexibility in the incorporation of this material system into a given architecture.

A scanning transmission electron microscopy electron energy loss spectroscopy (STEM-EELS) analysis was performed on all cross-sectional samples (Figure 5) with the hypothesis that a titanium deficiency due to either titanium vacancies or oxygen interstitials was the primary cause of the *p*-type behavior. The results indicate that the O:Ti ratio is consistently larger than 2 for all of the as-deposited conditions. For the O<sub>2</sub> annealing

conditions, the ratio does not begin to measurably decrease until 1000 °C and there it does so uniformly. However, for the N<sub>2</sub> annealing ambient, the top 4 nm of the film undergoes significant oxygen loss starting at 600 °C.

An XPS study was performed for additional verification of the STEM-EELS results. To minimize damage to the films, no argon sputtering or pretreatment of the samples was performed prior to the analysis. It is well-known that these processes can significantly alter the measured ratio of oxygen to titanium.<sup>30</sup> Instead, high resolution measurements were performed on unaltered surfaces and the amount of oxygen bonded to Ti<sup>4+</sup> was measured by fitting the oxygen signal to the distinct, chemically shifted peak of this particular bond. Even if additional oxygen was bonded to titanium that was not accounted for, we would still obtain a lower bound on the oxygen to titanium ratio of the film, which allows for an accurate characterization of titanium deficiency if that measured ratio was consistently greater than 2. The results from the XPS analysis (Figure S4, Supporting Information) indicate that the O:Ti ratio for the majority of the films is indeed greater than 2. The two notable exceptions are the 900 and 1000 °C annealing conditions for the 200 °C deposited sample set which also showed a carrier type inversion in the Hall effect measurements and significant surface oxygen loss from the EELS analysis. The as-deposited, nitrogen-doped sample also shows an O:Ti ratio greater than 2 but that can be attributed to the heavy doping compensating for the native *p*-type conductivity.

If the as-deposited ALD TiO<sub>2</sub> samples are titanium deficient, then there must also be a process by which that deficiency is corrected through the annealing because the hole concentration decreases with increasing annealing temperatures regardless of the annealing process gas. Because titanium vacancies in rutile crystals have been shown to be difficult to produce even with 900 °C annealing temperatures,<sup>21</sup> it is more likely that our low temperature ALD process results in a high concentration of oxygen interstitials that cause the *p*-type behavior. To address the question of what happens to the hypothesized excess oxygen, cross section TEM measurements were analyzed with a focus on the Si-TiO<sub>2</sub> interface (Figure 6). From Figure 6a, the

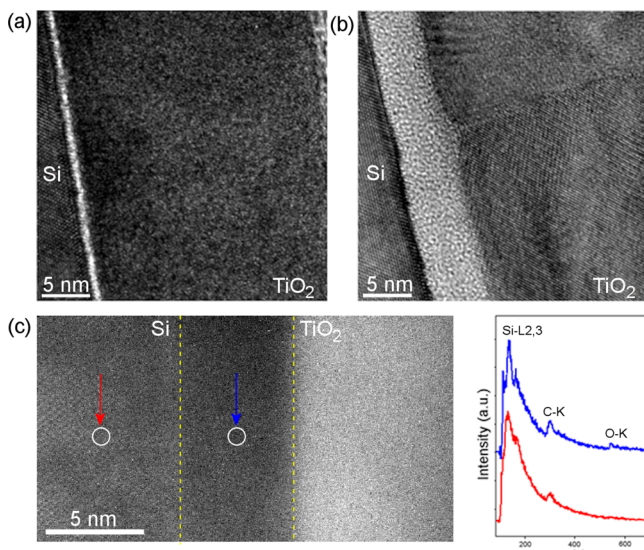


**Figure 6.** Bright field cross section TEM images of (a) as-deposited 250 °C ALD TiO<sub>2</sub>, (b) 1000 °C N<sub>2</sub> annealed 250 °C ALD TiO<sub>2</sub> and (c) Si-SiO<sub>x</sub>-TiO<sub>2</sub> interface with EELS spectra taken at the Si substrate and SiO<sub>x</sub> layer as denoted by the corresponding arrow color.

as-deposited sample is primarily amorphous with some small dispersed crystallites and a thin silicon oxide layer at the interface, as expected. The sample annealed at 1000 °C in nitrogen (Figure 6b) exhibits large crystalline TiO<sub>2</sub> grains and a much thicker interfacial silicon oxide layer. EELS analysis of the silicon substrate and interfacial layer (Figure 6c) confirms the SiO<sub>x</sub> composition based on the shape and shift of the Si-L<sub>2,3</sub> peak. It can be inferred that excess interstitial oxygen in the as deposited film migrates to the Si-TiO<sub>2</sub> interface and oxidizes portions of the silicon substrate. This process is accelerated by larger temperatures and we accordingly observe a gradual increase in the thickness of this interfacial silicon oxide layer with increasing annealing temperature. Because these samples were annealed in a pure nitrogen ambient, it is unlikely that the silicon oxidation was due to an external oxygen source. Moreover, as evidenced by the surface oxygen loss with N<sub>2</sub> annealing in Figure 5b, the ambient environment can also accept oxygen that is shed by the film.

To demonstrate the applicability of the results detailed above, TiO<sub>2</sub> homojunction diodes were fabricated by a lithography process on the same type of undoped FZ silicon

substrates, with the architecture depicted in Figure 7a. A 200 nm thick, lightly doped *p*-type TiO<sub>2</sub> layer was deposited at 250 °C then annealed for 20 min in O<sub>2</sub> at 500 °C to obtain a hole concentration of 10<sup>16</sup> cm<sup>-3</sup> and mobility of 400 cm<sup>2</sup>/(V·s). A portion of this *p*-type TiO<sub>2</sub> layer was then removed using a masked HF wet etch process and a layer of ALD Al<sub>2</sub>O<sub>3</sub> of the same thickness was deposited in its place with the intention of providing a geometrically well-defined homojunction interface. A 40 nm thick N:TiO<sub>2</sub> layer was then deposited on top with no additional postprocessing. Aluminum electrodes were evaporated 1 mm away from the TiO<sub>2</sub> *p-n* interface to prevent Al atom contamination of the junction.

The *i-V* behavior of the diode was measured and compared to an ideal model of the device simulated with the SCAPS-1D tool and incorporating the experimentally measured electrical properties of the TiO<sub>2</sub> layers. As shown in Figure 7b, there is a good correlation between the two results. The lower turn-on voltage of the measured device can be explained by the existence of a set of defect states at the interface of the two TiO<sub>2</sub> layers. Moreover, the nonideal slope of the measured *i-V* curve in the exponential increase region can be attributed to the series resistance of the device that was unaccounted for in the modeling. These differences aside, the ALD TiO<sub>2</sub> *p-n* diode exhibits high quality rectifying characteristics that can be employed in a number of device architectures.

## CONCLUSION

In conclusion, TiO<sub>2</sub> films were fabricated by ALD on undoped, highly resistive FZ silicon substrates at three different deposition conditions. These samples were subsequently annealed in a wide range of temperatures and characterized to ascertain their structural and electrical properties. Surprisingly, *p*-type conductivity was discovered in nearly all of the prepared samples and the dominant hypothesis regarding the source of this behavior is that a native excess of oxygen interstitials is present in the as-deposited film at all of the deposition conditions. This behavior of ALD TiO<sub>2</sub> or TiO<sub>2</sub> deposited by other methods has never been reported to date and to the best of our knowledge. Since significant effort has been made to dope TiO<sub>2</sub> to obtain *p*-type behavior, this discovery has the potential to provide a much simpler route to the same end goal. Moreover, it has been shown that the electrical characteristics of the *p*-type TiO<sub>2</sub> films can be varied across a wide range. This ability to tailor the properties of the film enhances its utility in a number of novel applications such as fully transparent TiO<sub>2</sub>

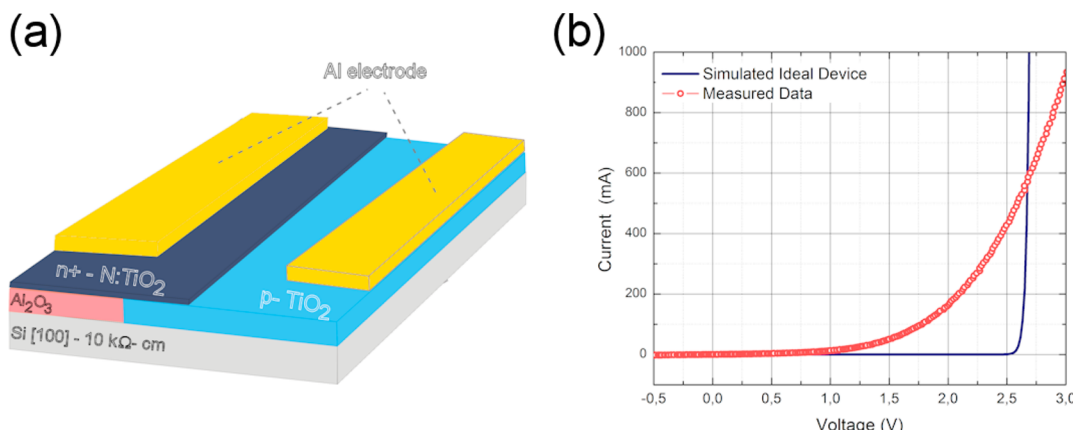


**Figure 7.** ALD TiO<sub>2</sub> homojunction diode: (a) device architecture and (b) dark *i-V* characteristics.

diodes, thin film transistors and solar cells as well as more traditional applications in photocatalysis and electrochemistry. As a demonstration, we fabricated the first reported ALD TiO<sub>2</sub> homojunction diode and confirmed that it exhibits excellent rectifying characteristics.

## ASSOCIATED CONTENT

### Supporting Information

SEM surface topography analysis; TEM cross section images and crystal structure analyses; XPS measured oxygen to titanium ratio versus annealing temperature. This material is available free of charge via the Internet at <http://pubs.acs.org>.

## AUTHOR INFORMATION

### Corresponding Author

\*A. T. Iancu. E-mail: andrei.iancu@stanford.edu. Tel.: 1-562-225-2463. Fax: 1-650-723-5034.

### Author Contributions

The paper was written through contributions of all authors. All authors have given approval to the final version of the paper.

### Notes

The authors declare no competing financial interest.

## ACKNOWLEDGMENTS

We thank Professor Joop Schoonman of TU Delft for his enlightening discussions and valuable feedback. We also thank Dr. Philip Van Stockum for his assistance in reviewing and editing the manuscript. Fabrication and analysis work was performed in part at the Stanford Nanofabrication Facility, the Stanford Nanocharacterization Lab and the Stanford Nano Center.

## REFERENCES

- (1) Weir, A.; Westerhoff, P.; Fabricius, L.; Hristovski, K.; Von Goetz, N. Titanium Dioxide Nanoparticles in Food and Personal Care Products. *Environ. Sci. Technol.* **2012**, *46*, 2242–2250.
- (2) Zhang, X.; Zhang, T.; Ng, J.; Sun, D. D. High-Performance Multifunctional TiO<sub>2</sub> Nanowire Ultrafiltration Membrane with a Hierarchical Layer Structure for Water Treatment. *Adv. Funct. Mater.* **2009**, *19*, 3731–3736.
- (3) Armelao, L.; Barreca, D.; Bottaro, G.; Gasparotto, A.; Maccato, C.; Maragno, C.; Tondello, E.; Lavrenčič, Š. U.; Bergant, M.; Mahne, D. Photocatalytic and Antibacterial Activity of TiO<sub>2</sub> and Au/TiO<sub>2</sub> Nanosystems. *Nanotechnology*. **2007**, *18*, 375709–375716.
- (4) Blossey, R. Self-Cleaning Surfaces — Virtual Realities. *Nat. Mater.* **2003**, *2*, 301–306.
- (5) Kim, S. K.; Kim, W. D.; Kim, K. M.; Hwang, C. S.; Jeong, J. High Dielectric Constant TiO<sub>2</sub> Thin Films on a Ru Electrode Grown at 250°C by Atomic-Layer Deposition. *Appl. Phys. Lett.* **2004**, *85*, 4112–4114.
- (6) Kim, S. K.; Choi, G. J.; Lee, S. Y.; Seo, M.; Lee, S. W.; Han, J. H.; Ahn, H. S.; Han, S.; Hwang, C. S. Al-Doped TiO<sub>2</sub> Films with Ultralow Leakage Currents for Next Generation DRAM Capacitors. *Adv. Mater.* **2008**, *20*, 1429–1435.
- (7) Kim, S. B.; Brown, S. L.; Rossnagel, S. M.; Bruley, J.; Copel, M.; Hopstaken, M. J. P. Oxygen Migration in TiO<sub>2</sub>-based Higher-k Gate Stacks. *J. Appl. Phys.* **2010**, *107*, 054102–054109.
- (8) Yang, J. J.; Strukov, D. B.; Stewart, D. R. Memristive Devices for Computing. *Nat. Nanotechnol.* **2013**, *8*, 13–24.
- (9) Kwon, D. H.; Kim, K. M.; Jang, J. H.; Jeon, J. M.; Lee, M. H.; Kim, G. H.; Li, X. S.; Park, G. S.; Lee, B.; Han, S.; Kim, M.; Hwang, C. S. Atomic Structure of Conducting Nanofilaments in TiO<sub>2</sub> Resistive Switching Memory. *Nat. Nanotechnol.* **2010**, *5*, 148–153.
- (10) Yang, J. J.; Pickett, M. D.; Xuema, L.; Ohlberg, D. A. A.; Stewart, D. R.; Williams, R. S. Memristive Switching Mechanism for Metal/Oxide/Metal Nanodevices. *Nat. Nanotechnol.* **2008**, *3*, 429–433.
- (11) Chen, Y. W.; Prange, J. D.; Dühnen, S.; Park, Y.; Gunji, M.; Chidsey, C. E. D.; McIntyre, P. C. Atomic Layer-Deposited Tunnel Oxide Stabilizes Silicon Photoanodes for Water Oxidation. *Nat. Mater.* **2011**, *10*, 539–544.
- (12) Lin, F.; Boettcher, S. W. Adaptive Semiconductor/Electrocatalyst Junctions in Water-Splitting Photoanodes. *Nat. Mater.* **2014**, *13*, 81–86.
- (13) He, Y.; Tilcock, A.; Dulub, O.; Selloni, A.; Diebold, U. Local Ordering and Electronic Signatures of Submonolayer Water on Anatase TiO<sub>2</sub>(101). *Nat. Mater.* **2009**, *8*, 585–589.
- (14) Varghese, O. K.; Paulose, M.; Grimes, C. A. Long Vertically Aligned Titania Nanotubes on Transparent Conducting Oxide for Highly Efficient Solar Cells. *Nat. Nanotechnol.* **2009**, *4*, 592–597.
- (15) Liu, M.; Johnston, M. B.; Snaith, H. J. Efficient Planar Heterojunction Perovskite Solar Cells by Vapor Deposition. *Nature*. **2013**, *501*, 395–398.
- (16) Burschka, J.; Pellet, N.; Moon, S. J.; Baker, R. H.; Gao, P.; Nazeeruddin, M. K.; Grätzel, M. Sequential Deposition as a Route to High-Performance Perovskite-Sensitized Solar Cells. *Nature*. **2013**, *499*, 316–319.
- (17) Ruiz, A.; Cornet, A.; Sakai, G.; Shimanoe, K.; Morante, J. R.; Yamazoe, N. Preparation of Cr-Doped TiO<sub>2</sub> Thin Films of p-Type Conduction for Gas Sensor Application. *Chem. Lett.* **2002**, *9*, 892–893.
- (18) Li, X.; Wu, S.; Hu, P.; Xing, X.; Liu, Y.; Yu, Y.; Yang, M.; Lu, Y. Structures and Magnetic Properties of p-Type Mn:TiO<sub>2</sub> Dilute Magnetic Semiconductor Thin Films. *J. Appl. Phys.* **2009**, *106*, 043913–043916.
- (19) Wang, Z.; Wang, W.; Tang, J.; Tung, L. D.; Spinu, L.; Zhou, W. Extraordinary Hall Effect and Ferromagnetism in Fe-Doped Reduced Rutile. *Appl. Phys. Lett.* **2003**, *83*, 518–521.
- (20) Das, S.; Liu, D.; Park, J. B.; Hahn, Y. B. Metal-Ion Doped p-Type TiO<sub>2</sub> Thin Films and Their Applications for Heterojunction Devices. *J. Alloys Compd.* **2013**, *553*, 188–193.
- (21) Nowotny, M. K.; Bak, T.; Nowotny, J.; Sorrell, C. C. Titanium Vacancies in Nonstoichiometric TiO<sub>2</sub> Single Crystal. *Phys. Status Solidi B* **2005**, *242*, R88–R90.
- (22) Nowotny, J.; Bak, T.; Burg, T. Electrical Properties of Polycrystalline TiO<sub>2</sub> at Elevated Temperatures - Electrical Conductivity. *Phys. Status Solidi B* **2007**, *244*, 2037–2054.
- (23) Nowotny, J.; Bak, T.; Burg, T. Electrical Properties of Polycrystalline TiO<sub>2</sub> - Prolonged Oxidation Kinetics. *Ionics*. **2007**, *13*, 79–82.
- (24) Irie, H.; Washizuka, S.; Watanabe, Y.; Kako, T.; Hashimoto, K. Photoinduced Hydrophilic and Electrochemical Properties of Nitrogen-Doped TiO<sub>2</sub> Films. *J. Electrochem. Soc.* **2005**, *152*, E351–E356.
- (25) Katamreddy, R.; Omarjee, V.; Feist, B.; Dussarrat, C. Ti Source Precursors for Atomic Layer Deposition of TiO<sub>2</sub>, STO and BST. *ECS Trans.* **2008**, *16*, 113–122.
- (26) Li, J. G.; Ishigaki, T. Brookite → Rutile Phase Transformation of TiO<sub>2</sub> Studied with Monodispersed Particles. *Acta Mater.* **2004**, *52*, 5143–5150.
- (27) Zhang, H. Z.; Banfield, J. F. Understanding Polymorphic Phase Transformation Behavior during Growth of Nanocrystalline Aggregates: Insights from TiO<sub>2</sub>. *J. Phys. Chem. B* **2000**, *104*, 3481–3487.
- (28) Kholmanov, I. N.; Barborini, E.; Vinati, S.; Piseri, P.; Podestà, A.; Ducati, C.; Lenardi, C.; Milani, P. The Influence of the Precursor Clusters on the Structural and Morphological Evolution of Nanostructured TiO<sub>2</sub> under Thermal Annealing. *Nanotechnology*. **2003**, *14*, 1168–1173.
- (29) Martin, N.; Rousselot, C.; Rondot, D.; Palmino, F.; Mercier, R. Microstructure Modification of Amorphous Titanium Oxide Thin Films during Annealing Treatment. *Thin Solid Films*. **1997**, *300*, 113–121.
- (30) Hashimoto, S.; Tanaka, A.; Murata, A.; Sakurada, T. Formulation for XPS Spectral Change of Oxides by Ion Bombardment as a Function of Sputtering Time. *Surf. Sci.* **2004**, *556*, 22–32.